Supporting Information

Donor-Acceptor Duality of The Transition-Metal-Like B_2 Core in Core-Shell-Like Metallo-Borospherenes $La_3\&[B_2@B_{17}]^-$ and $La_3\&[B_2@B_{18}]^-$

Xiao-Yun Zhao,[a,b] Miao Yan,[a] Zhihong Wei,*[a] and Si-Dian Li*[a]

[a] Key Laboratory of Materials for Energy Conversion and Storage of Shanxi Province, Institute of Molecular Science, Shanxi University, Taiyuan 030006, China.

[b] Department of Applied Chemistry, Yuncheng University, Yuncheng 044000, China.

E-mail: lisidian@sxu.edu.cn

Contents

Fig. S1 Low-lying isomers of $La_3B_{20}^-$ with their relative energies (with zero-point corrections included) indicated in eV at PBE0/B/6-311+G*/La/ECP28MWB, TPSSH/B/6-311+G*/La/ECP28MWB (in brackets) and CCSD(T)/B/6-31G*/La/ECP28MWB //PBE0/ B/6-311+G*/La/ECP28MWB (in square brackets) levels. The B_n cores are highlighted in red.

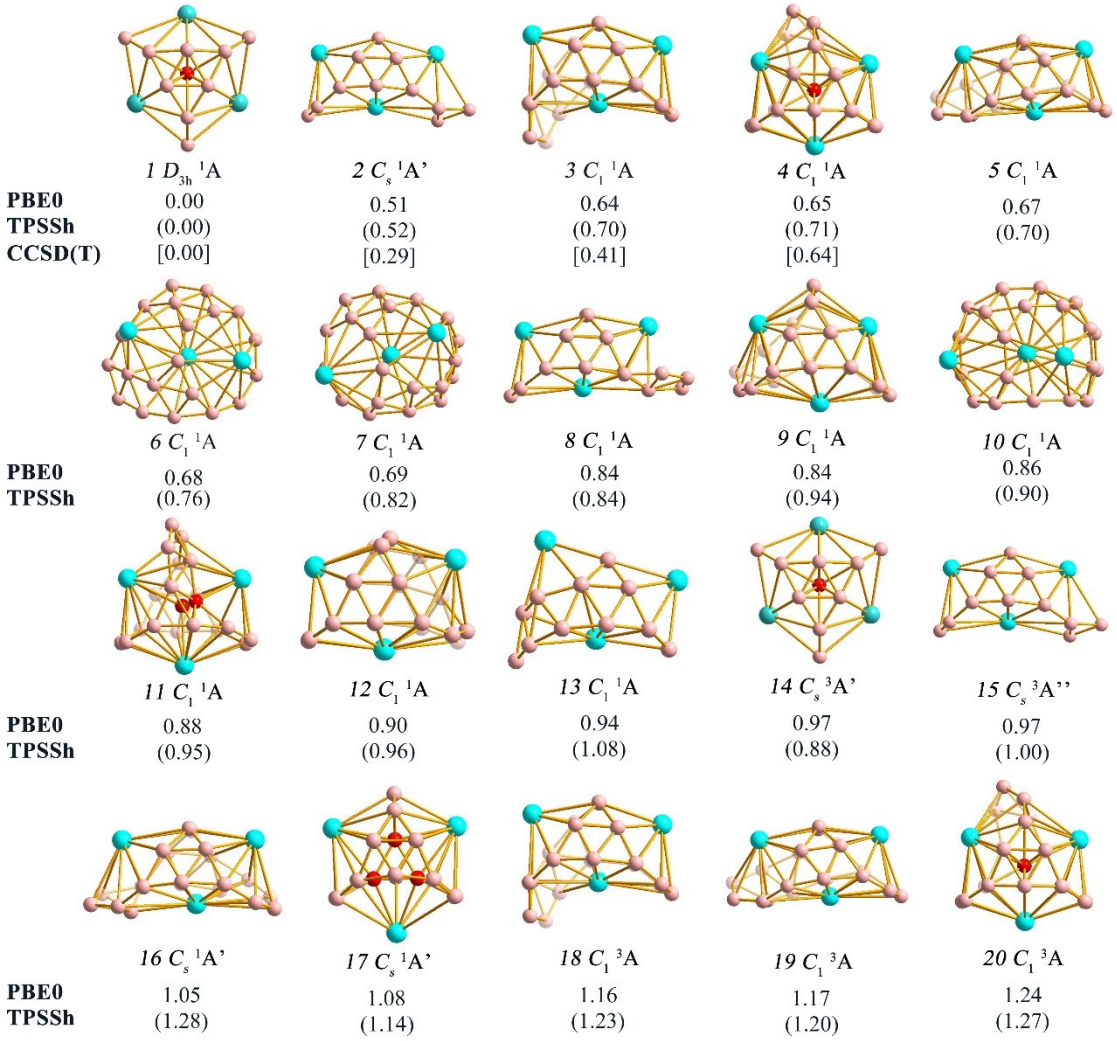

Fig. S2 Low-lying isomers of $La_3B_{19}^-$ with their relative energies (with zero-point corrections included) indicated in eV at PBE0/B/6-311+G*/La/ECP28MWB, TPSSh/B/6-311+G*/La/ECP28MWB (in brackets) and CCSD(T)/B/6-31G*/La/ECP28MWB //PBE0/ B/6-311+G*/La/ECP28MWB (in square brackets) levels. The B_n cores are highlighted in red.

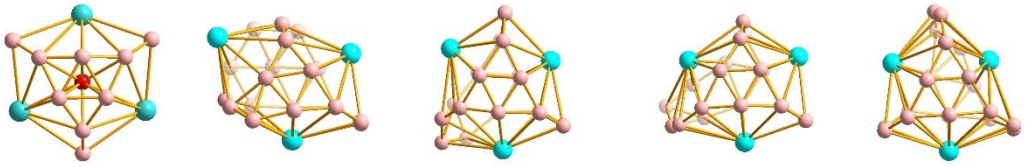

	1 C_{2v} $^2A_1$	*2* C_1 ^2A	*3* C_1 ^2A	*4* C_1 ^2A	*5* C_2 ^2A
PBE0	0.00	0.51	0.55	0.86	0.87
TPSSh	(0.00)	(0.83)	(0.69)	(0.98)	(0.83)
CCSD(T)	[0.00]	[0.65]	[0.20]		

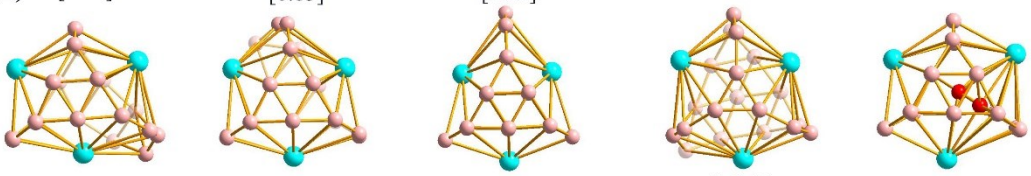

	6 C_1 ^2A	*7* C_1 ^2A	*8* C_s $^2A'$	*9* C_1 ^2A	*10* C_1 ^2A
PBE0	0.97	0.98	1.05	1.11	1.13
TPSSh	(1.06)	(1.08)	(0.95)	(1.27)	(1.17)

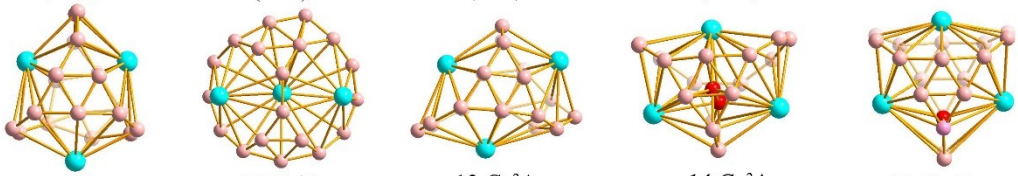

	11 C_1 ^2A	*12* C_1 ^2A	*13* C_1 ^2A	*14* C_1 ^2A	*15* C_{2v} $^2B_1$
PBE0	1.24	1.22	1.29	1.33	1.47
TPSSh	(1.37)	(1.09)	(1.43)	(1.18)	(1.58)

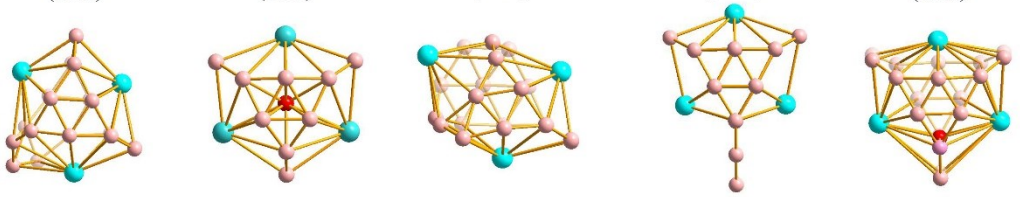

	16 C_1 ^4A	*17* C_{2v} $^4A_1$	*18* C_1 ^4A	*19* C_{2v} $^4B_2$	*20* C_{2v} $^4A_1$
PBE0	1.61	1.65	1.83	2.45	2.81
TPSSh	(1.72)	(1.59)	(1.88)	(2.42)	(2.83)

Fig. S3 Born-Oppenheimer molecular dynamics simulations of C_{2v} La_3&$[B_2@B_{17}]^-$ (**2**) at 300K, 700K and 1000K, with the calculated average root-mean-square-deviations (RMSD) and maximum bond length deviations (MAXD) indicated in Å.

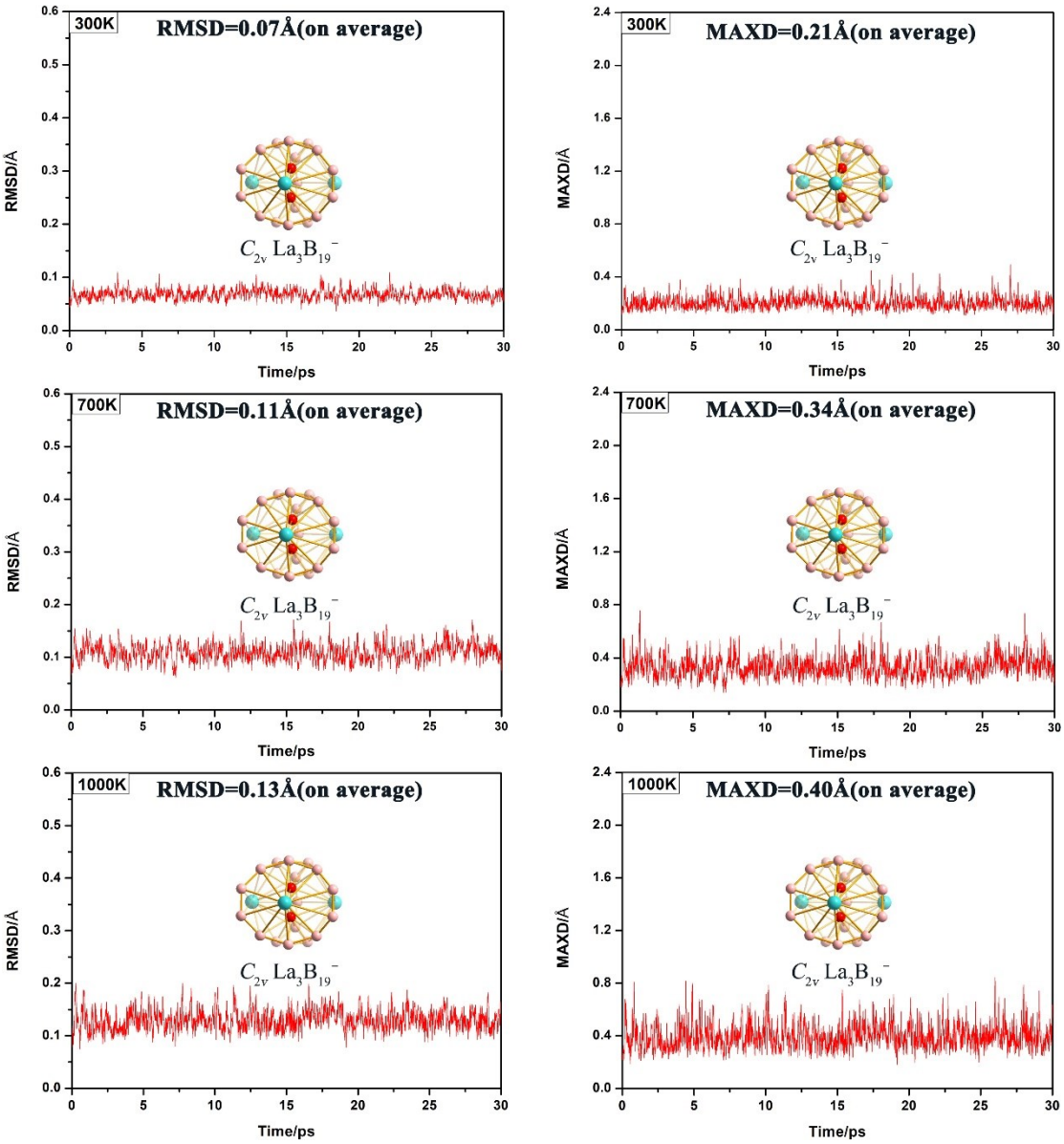

Fig. S4 Born-Oppenheimer molecular dynamics simulations of D_{3h} La_3&$[B_2@B_{18}]^-$ (**3**) at 300K, 700K and 1000K, with the calculated average root-mean-square-deviations (RMSD) and maximum bond length deviations (MAXD) indicated in Å.

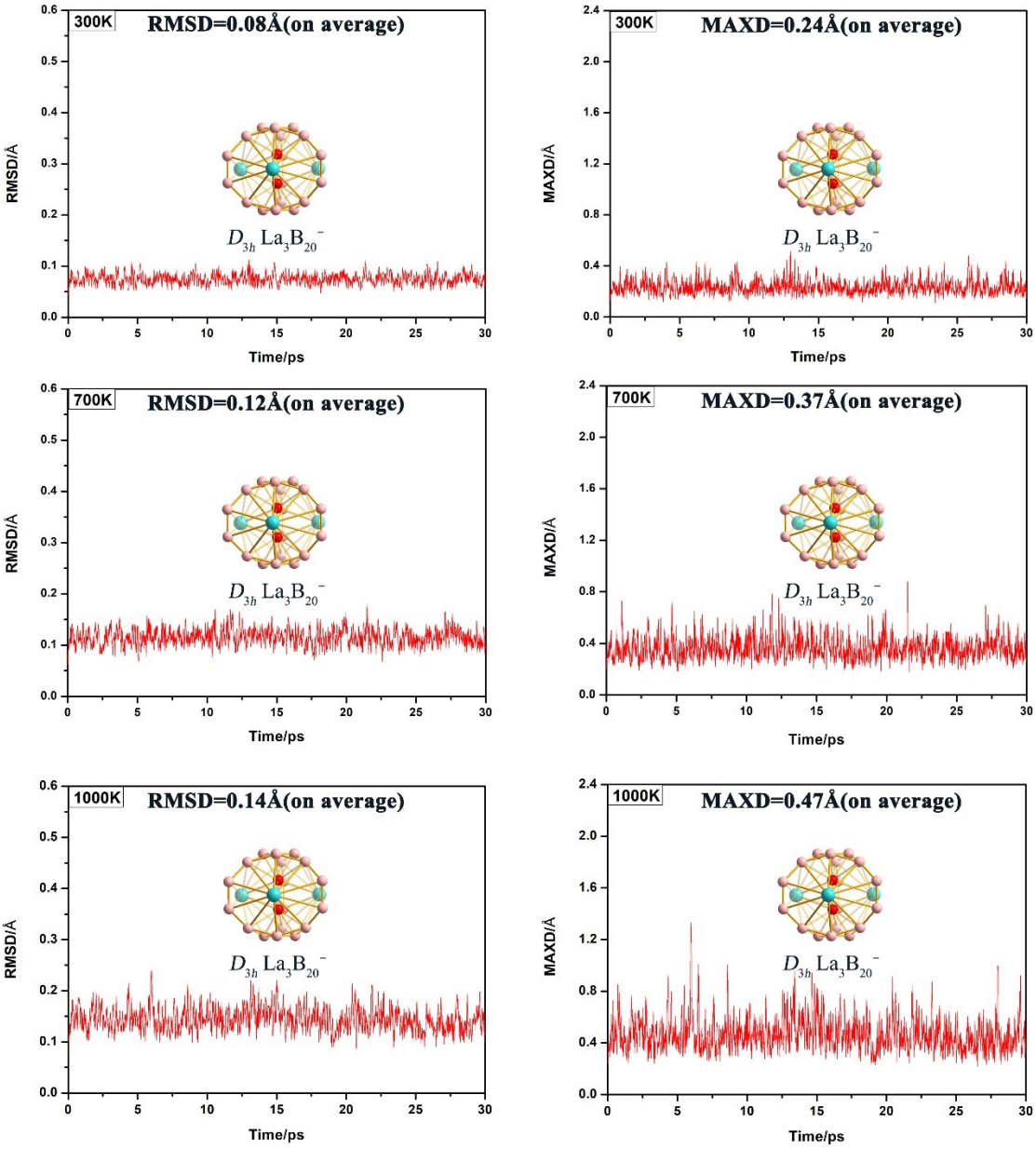

Fig. S5. Shape of the deformation densities $\Delta\rho_{(1)-(4)}$ (isovalue = 0.0025 a.u.) and eigenvalues ν, which are associated with the orbital interactions $\Delta E_{orb(1)-(4)}$ in $B_{20}La_3^-$. The color code of the charge flow is red → blue.

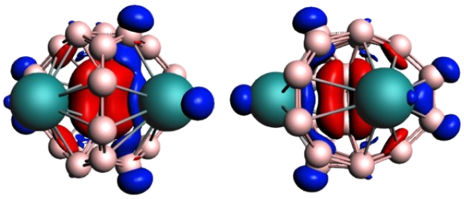

(a) $\Delta\rho_{(1)}$ (ν = 1.27)
$\Delta E_{orb(1)}$ = -157.7 kcal mol^{-1} (×2)

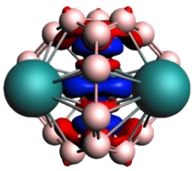

(c) $\Delta\rho_{(3)}$ (ν = 0.89)
$\Delta E_{orb(3)}$ = -139.3 kcal mol^{-1}

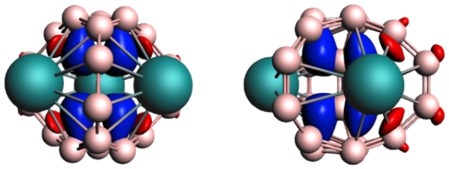

(b) $\Delta\rho_{(2)}$ (ν = 0.73)
$\Delta E_{orb(2)}$ = -63.8 kcal mol^{-1} (×2)

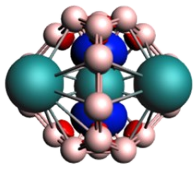

(d) $\Delta\rho_{(4)}$ (ν = 0.61)
$\Delta E_{orb(4)}$ = -79.1 kcal mol^{-1}

Fig. S6 AdNDP bonding patterns of C_{2v} La_3&$[B_2@B_{17}]^{2-}$, with the occupation numbers (ON) indicated.

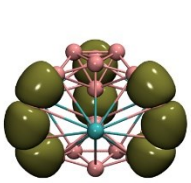

8 2c-2e B_2 σ bonds
ON = 1.85-1.88 |e|

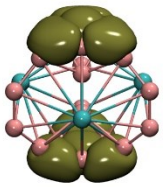

8 3c-2e B_3 σ bonds
ON = 1.72-1.90 |e|

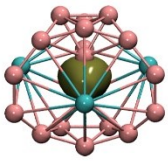

1 2c-2e B_2 σ bonds
ON = 1.70 |e|

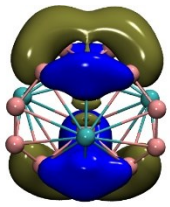

2 7c-2e $B_6(\pi)$-B(σ) bonds
ON = 1.81 |e|

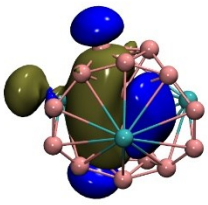

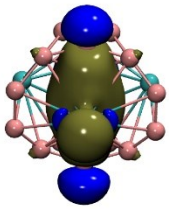

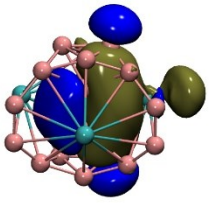

3 5c-2e $B_4(\pi)$-La(d_σ) bonds
ON = 1.66-1.69 |e|

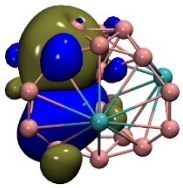

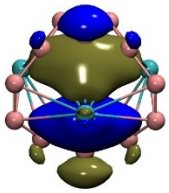

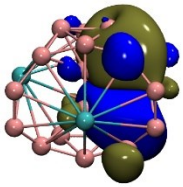

2 12c-2e $B_{11}(\pi)$-La(d_π) bonds
1 13c-2e $B_{12}(\pi)$-La(d_π) bonds
ON = 1.73-1.77 |e|

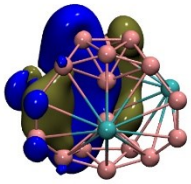

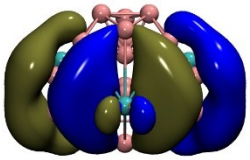

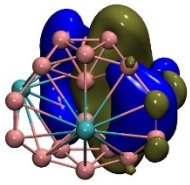

2 12c-2e $B_{11}(\pi)$-La(d_π) bonds
1 13c-2e $B_{12}(\pi)$-La(d_π) bonds
ON = 1.84-87 |e|

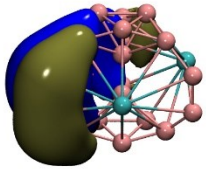

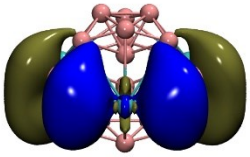

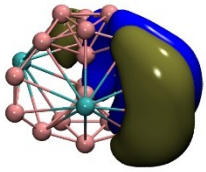

2 12c-2e $B_{11}(\pi)$-La(d_σ) bonds
1 13c-2e $B_{12}(\pi)$-La(d_σ) bonds
ON = 1.86-1.89 |e|

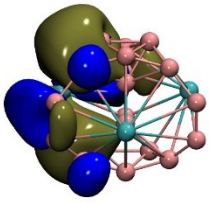

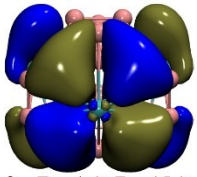

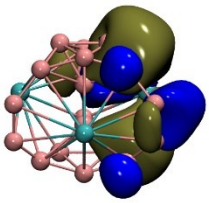

2 12c-2e $B_{11}(\pi)$-La(d_δ) bonds
1 13c-2e $B_{12}(\pi)$-La(d_δ) bonds
ON = 1.64-1.67 |e|

Fig. S7 Comparison of the calculated iso−chemical shielding surfaces (ICSSs) of (a) C_{2v} La_3&$[B_2@B_{17}]^-$ (**2**), (b) D_{3h} La_3&$[B_2@B_{18}]^-$ (**3**), and (c) D_{6h} C_6H_2, with the corresponding NICS−ZZ components indicated. The C_2 axis of La_3&B_{19}^- and La_3&B_{20}^- are designated as z axis in vertical direction. Yellow regions stand for chemical shielding areas, while green areas represent chemical de-shielding areas.

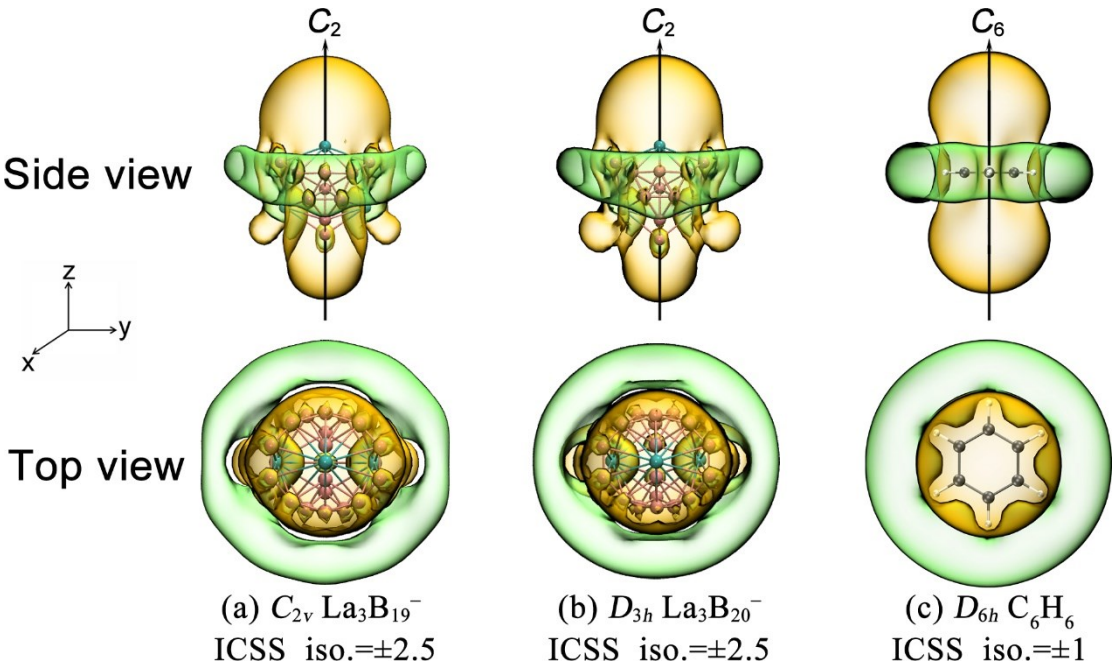

Fig. S8 Simulated (a) IR, (b) Raman and (c) photoelectron spectrum of C_{2v} La_3&$[B_2@B_{17}]^-$ (**2**) at PBE0/B/6-311+G*/La/ECP28MWB level.

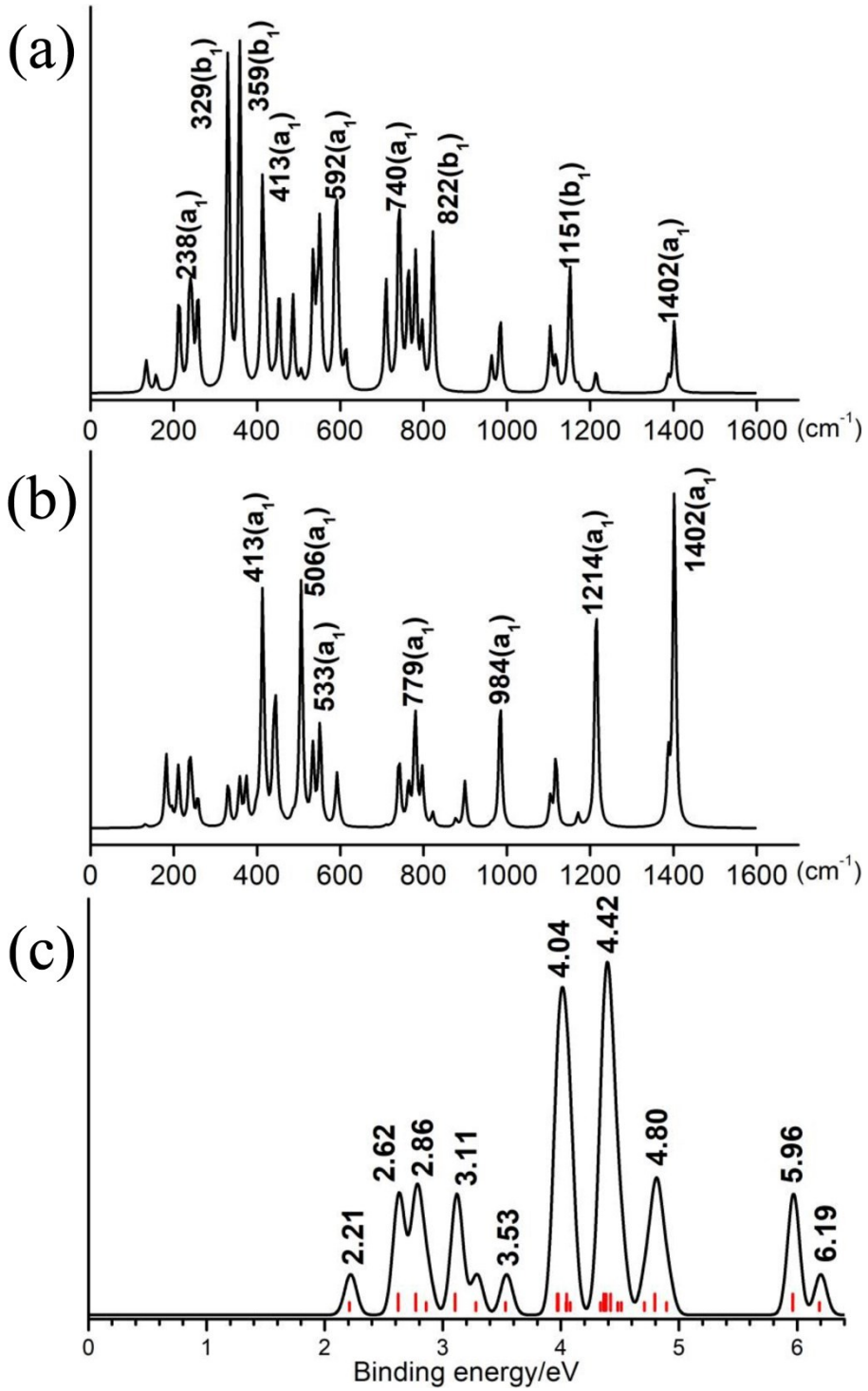

Fig. S9 Simulated (a) IR and (b) Raman spectrum of D_{3h} La_3&B_{18}^- at PBE0/B/6-311+G*/La/ECP28MWB level.

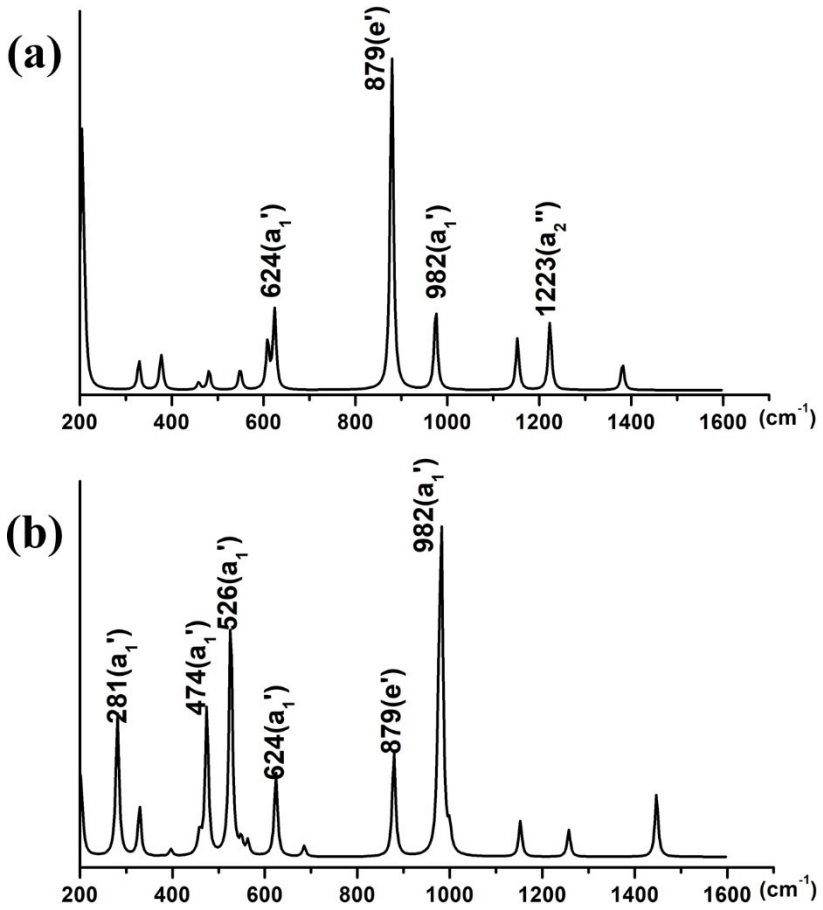

Table S1. Calculated natural atomic charges, electronic configurations, and Wiberg bond orders of the concerned atoms or structural units in C_{2v} La_3&$[B_2@B_{17}]^-$ (**2**) and D_{3h} La_3&$[B_2@B_{18}]^-$ (**3**).

	Natural Charge				Electron Configuration	
	La	B_{core}	B_6	B_{edge}	La	B_{core}
$B_{19}La_3^-$	1.20 1.29	–0.10	–0.21 - –0.25	–0.33 –0.14	$[Xe]6s^{0.11}5d^{1.53}$ $[Xe]6s^{0.12}5d^{1.43}$	$[H]2s^{0.47}2p^{2.58}$
$B_{20}La_3^-$	1.28	–0.13	–0.23 - –0.25	–0.29	$[Xe]6s^{0.12}5d^{1.46}$	$[H]2s^{0.48}2p^{2.60}$
	Wiberg bond index					
	La_{total}	B_{total}	B_{core}-B_{core}	La-B_{core}	La-B_{ring}	B_{core}-B_6
$B_{19}La_3^-$	3.15 3.22	3.60 3.82	0.73	0.27	0.17-0.26	0.27-0.42
$B_{20}La_3^-$	3.11	3.71 3.85	0.73	0.26	0.16-0.29	0.27-0.43

Table S2. EDA-NOCV calculations using using different fragments as well as different electron configurations at PBE0/TZP-ZORA level for D_{3h} La_3&$[B_2@B_{18}]^-$ (**3**). All energy values are in kcal mol^{-1}.

Energy terms	Interacting fragments				
	B_2 $[^1\Sigma_g^+]$ + $B_{18}La_3^-$	B_2 $[^3\Sigma_g^-]$ + $B_{18}La_3^-$	B_2^- + $B_{18}La_3$	B_{20}^- + La_3	B_{20} + La_3^-
ΔE_{int}	-349.9	-276.78	-354.7	-645.46	-701.72
ΔE_{Pauli}	1053.5	1402.39	1653.08	2147.44	2270.48
ΔE_{elstat}	-685.5	-699.47	-1107.07	-1297.06	-1366.45
ΔE_{orb}	-717.9	-979.7	-900.71	-1495.84	-1605.75

Table S3. The compositions from the B_2 $[^1\Sigma_g^+]$ and $B_{18}La_3^-$ $[^1A_1]$ fragments to the 29e′, 15e″, 22a_1′ and 13a_2″ MOs of D_{3h} La_3&$[B_2@B_{18}]^-$ (**3**).

MOs	Compositions
29e′	33% ($B_{18}La_3^-$ 29e′) + 26% ($B_{18}La_3^-$ 27e′) + 16% (B_2 1e′)
15e″	76% ($B_{18}La_3^-$ 15e″) + 15% (B_2 1e″)
22a_1′	32% ($B_{18}La_3^-$ 20a_1′) + 21% ($B_{18}La_3^-$ 19a_1′) + 25% (B_2 3a_1′)
13a_2″	70% ($B_{18}La_3^-$ 12a_2″) + 20% ($B_{18}La_3^-$ 10a_2″) + 25% (B_2 2a_2″)

Table S4 Optimized coordinates of C_{2v} La_3&$[B_2@B_{17}]^-$ (**2**) at PBE0.

B	0.000000	0.816066	-0.132664
B	0.876134	2.201706	-0.723996
B	0.000000	2.331682	0.796152
B	-1.585405	1.845301	0.773170
B	-2.572700	0.754338	1.416424
B	0.000000	-2.331682	0.796152
B	-0.876134	-2.201706	-0.723996
B	1.585405	1.845301	0.773170
B	2.572700	-0.754338	1.416424
B	2.572700	0.754338	1.416424
B	0.000000	0.000000	-2.773172
B	0.000000	-0.816066	-0.132664
B	1.585405	-1.845301	0.773170
B	0.876134	-2.201706	-0.723996
B	0.000000	-1.400189	-1.924255
B	0.000000	1.400189	-1.924255
La	0.000000	0.000000	2.337690
La	2.325484	0.000000	-1.193743
La	-2.325484	0.000000	-1.193743
B	-1.585405	-1.845301	0.773170
B	-0.876134	2.201706	-0.723996
B	-2.572700	-0.754338	1.416424

Table S5 Optimized coordinates of D_{3h} La_3&$[B_2@B_{18}]^-$ (**3**) at PBE0.

B	-0.867337	-0.500757	2.276031
B	0.867337	-0.500757	2.276031
B	1.608320	0.928564	1.832823
B	-1.608320	0.928564	1.832823
B	-2.613217	1.508742	0.754202
B	0.000000	1.001515	-2.276031
B	-0.867337	-0.500757	-2.276031
B	0.000000	1.001515	2.276031
B	2.613217	1.508742	-0.754202
B	2.613217	1.508742	0.754202
B	0.000000	-3.017483	-0.754202
B	-1.608320	0.928564	-1.832823
B	1.608320	0.928564	-1.832823
B	0.867337	-0.500757	-2.276031
B	0.000000	-1.857128	-1.832823
B	0.000000	-1.857128	1.832823
La	0.000000	2.499282	0.000000
La	2.164442	-1.249641	0.000000
La	-2.164442	-1.249641	0.000000
B	-2.613217	1.508742	-0.754202
B	0.000000	-3.017483	0.754202
B	0.000000	0.000000	0.817146
B	0.000000	0.000000	-0.817146

Table S6 Optimized coordinates of D_{3h} $La_3B_{18}^-$ (**1**) at PBE0.

B	0.000000	0.956419	2.303950
B	0.828283	-0.478210	2.303950
B	0.000000	-1.877631	1.915718
B	-1.626076	0.938815	1.915718
B	-2.537306	1.464914	0.766682
B	-0.828283	-0.478210	-2.303950
B	0.000000	0.956419	-2.303950
B	-0.828283	-0.478210	2.303950
B	0.000000	-2.929828	-0.766682
B	0.000000	-2.929828	0.766682
B	2.537306	1.464914	-0.766682
B	-1.626076	0.938815	-1.915718
B	0.000000	-1.877631	-1.915718
B	0.828283	-0.478210	-2.303950
B	1.626076	0.938815	-1.915718
B	1.626076	0.938815	1.915718
La	-2.006402	-1.158397	0.000000
La	2.006402	-1.158397	0.000000
La	0.000000	2.316794	0.000000
B	-2.537306	1.464914	-0.766682
B	2.537306	1.464914	0.766682